EAEF Engineering in Agriculture, Environment and Food published by AABEA
Research Paper

EAEF XX(X) : X-X, 20XX

Efficient Searching for Grain Storage Container by Combine Robot*

Hiroki KURITA*1, Michihisa IIDA*2, Masahiko SUGURI*3, Ryohei MASUDA*3, Wonjae CHO*1

Abstract

In this study, a combine robot was equipped with an autonomous grain container searching function. In order to realize automated grain unloading, the combine robot has to search and identify the grain storage container in an outdoor environment. A planar board was attached to the container. The marker was searched for using a camera mounted on the unloading auger of the combine. An efficient marker searching procedure was proposed on the basis of a numerical analysis of the camera's field of view and was verified experimentally. The results showed that the combine robot efficiently searched for and detected the marker and positioned its spout at the target point over the container to unload the grain.

[Keywords] head-feeding combine robot, grain unloading operation, grain container searching operation, spout positioning, field of view

I Introduction

In Japan, the number of workers engaged in agriculture is decreasing, and the average age of agricultural workers is rapidly increasing. Food self-sufficiency in Japan remains low compared to other developed countries. Japan must improve its agricultural productivity in order to maintain its sustainability. Field robots are expected to play an important role in improving the efficiency of agricultural operations and meeting workforce shortages. Attempts to develop automated agricultural machinery have previously been reported (Noguchi and Terao, 1997; Ishida *et al*., 1998; Nagasaka *et al*., 2004; Takai *et al*., 2010). In a previous study (Iida *et al*., 2012), we robotized a head-feeding combine harvester (hereafter referred to as a combine) and used it to harvest rice and wheat in fields. The combine robot successfully traveled along a target path and harvested rice crops autonomously.

However, a human operator is needed to manually control the combine and unload grain from its grain tank into a separate grain storage container. We aimed to automate the unloading operation as well. A pickup truck is driven and parked by a human driver on a farm road. The parking position of the truck is determined in advance. As the combine robot can obtain this parking position as Global Positioning Satellite (GPS) data, it autonomously travels to a position near the truck when the grain tank is full. However, the position of the combine relative to the pickup truck is not strictly fixed, because the human driver cannot perfectly park the pickup truck without positional errors. Thus, the combine robot has to find the pickup truck by an image processing technique and then correct its relative position to unload grain into the truck without any loss.

Kurita *et al*. (2012) utilized an image processing technique to appropriately position the unloading auger to unload grain. Figure 1 shows the assumed situation for their concept.

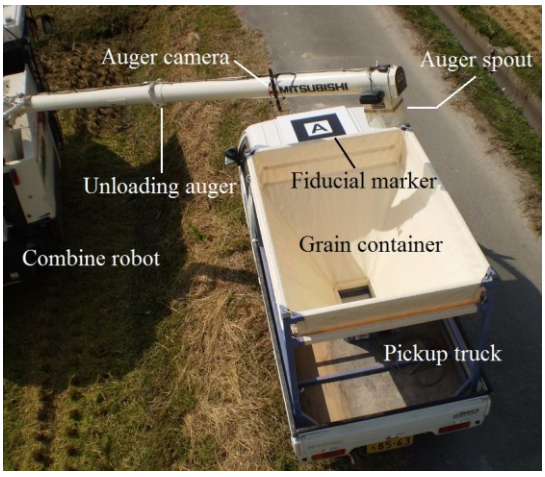

Fig. 1. Setup of autonomous unloading operation.

* Partly presented at the 6th International Symposium on Machinery and Mechatronics for Agricultural and Biosystems Engineering ISMAB 2012
*1 JSAM Student Member, Graduate School of Agriculture, Kyoto University, Kitashirakawa Oiwake-cho, Sakyo-ku, Kyoto, 606-8502, Japan
*2 JSAM Member, Corresponding author, Graduate School of Agriculture, Kyoto University, Kitashirakawa Oiwake-cho, Sakyo-ku, Kyoto, 606-8502, Japan ; iida@elam.kais.kyoto-u.ac.jp
*3 JSAM Member, Graduate School of Agriculture, Kyoto University, Kitashirakawa Oiwake-cho, Sakyo-ku, Kyoto, 606-8502, Japan

A planar fiducial marker (aluminum board, 400 mm × 400 mm) is placed on the roof of the pickup truck to detect the position of the grain container. The position is extracted from images captured by the camera attached to the unloading auger. On the basis of the extracted image features, the positional relation between the combine and container is determined using image processing techniques. The experimental results showed that the auger spout can be visually positioned at the target point with sufficient accuracy. In addition to this basic concept, the combine robot is required to search for and detect the fiducial marker autonomously and accurately.

Another issue with searching for the marker is work efficiency. Because work efficiency is one of the most important concerns for the automation of agricultural machinery (Buckmaster and Hilton, 2005), agricultural operations using an autonomous machine should not take much longer than the time required to perform the same operation manually. Thus, the autonomous unloading system should be designed in such a manner that the fiducial marker can be located smoothly and integrated into the autonomous unloading operation as quickly as possible.

For efficiently locating a grain container, a camera is required to smoothly capture the fiducial marker. A combine robot should search for the marker so that the camera can sweep over as wide an area as possible without overlapping. Thus, the strategy for efficient marker searching is closely linked to the camera's field of view (FOV) and its coverage. In visual servoing, the coverage of the camera's FOV is quite important for optimal control of a robot vehicle or manipulator; therefore, it has been widely studied by researchers concerned with mobile robots (Zhang and Ostrowski, 2002; Salaris *et al*., 2011), especially those who have developed a robot that searches for a particular object (Tsotsos and Shubina, 2007). It is difficult to actually measure the FOV of the auger camera for any set of decisive parameters, while a numerical simulation can give the FOV for any parameter with ease. Thus, the objectives of this study were as follows: to compute the FOV of the auger camera against FOV parameters based on the pinhole camera model, propose a marker searching algorithm in order to efficiently search for and accurately detect the marker and examine the actual performance of the proposed method with a combine robot.

II Materials and Methods

1. Kinematic Modeling and Mechanics of Unloading Auger

The test vehicle was a head-feeding combine harvester, VY50 CLAM (Mitsubishi Agricultural Machinery Co., Ltd, Shimane, Japan). The unloading auger of the combine was modeled with a two-degrees-of-freedom manipulator consisting of two joints (joints 1 and 2). As illustrated in Fig. 2, a right-handed coordinate system was assigned to the combine; the *x* axis of the coordinate system was along the body of the combine in the direction opposite to the direction of its motion, and the *z* axis pointed vertically upward. The state of the unloading auger was determined by the two joint angles (hereafter θ_1 and θ_2). Joint 1 rotated at an angle of $-110° < \theta_1 < 200°$. The grain could be discharged when $-110° < \theta_1 < 90°$. However, unloading was expected to be performed when $20° < \theta_1 < 90°$. Joint 2 rotated at an angle of $0° < \theta_2 < 45°$.

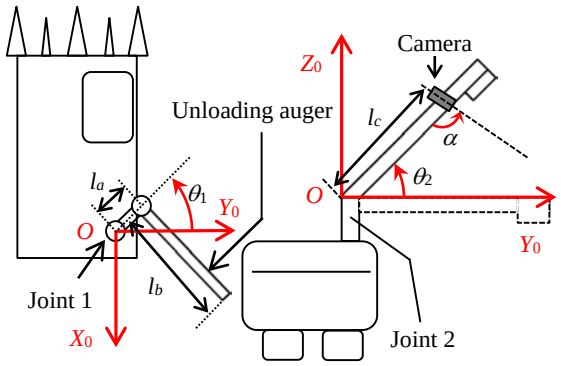

Fig. 2. Kinematic model of unloading auger.

Joints 1 and 2 were actuated by a DC motor and hydraulic cylinder, respectively. Each joint rotated at a constant rate: 38.3 °/s for joint 1 and 20.7 °/s (upward) and 10.7 °/s (downward) for joint 2 with on-off control. Link lengths l_a, l_b, and l_c were defined as shown in Fig. 2. The camera's elevation angle α was set to 71°. Table 1 lists the specifications of the camera.

Table 1. Camera specifications.

Model	UCAM-DLA200H (ELECOM)
Image sensor	1/4 in CMOS
Focal length	4.3 mm
F-number	1.8
Angle of view (diagonal)	60 °

2. FOV of Auger Camera

A rice paddy is usually enclosed by embankments and at least one farm road (see Fig. 3).

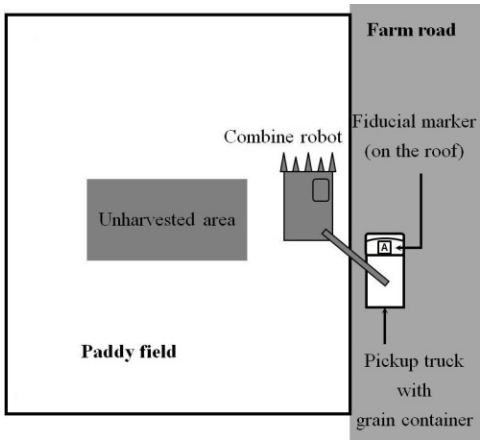

Fig. 3. Positional relation between the combine and the truck.

A commercialized head-feeding combine harvester is equipped with its unloading auger on the right side of the vehicle (see Fig. 3). As is the case for manned harvesting, the combine robot harvests rice crops in an anticlockwise fashion (Iida *et al*., 2012). Thus, in this study, the truck was always located on the right side of the combine. Let h_{fr} be the height of the adjacent farm road from a paddy field, h_c be the height of joint 1 of the combine harvester, and h_{kt} be the height of the pickup truck.

In general, the FOV can be represented by its angle of view (AOV) and depth of field (DOF). The AOV comprises the vertical and horizontal AOV. The DOF represents the area of the visual scene that is acceptably sharp. Outside of this range, images are blurred. The DOF depends on the focal length of the camera. In this study, the focal length of the camera was kept constant so that the DOF would fall within an acceptable range of sharpness. The DOF was empirically determined; at the same time, the target plane (i.e., the roof of the truck) was experimentally confirmed to form an image with sufficient sharpness for the expected range of the height from the paddy field to the farm road h_{fr}. In this study, the range was assumed to be 0 m < h_{fr} < 1.5 m.

A pinhole camera model (Gonzalez and Wintz, 1987; Xu and Zhang, 1996) was adopted for the following simulation. Further approximations were applied to the system model. In the following analysis, the unloading auger was dealt with as a line, not a solid object, and the camera's dimensions were neglected. Hence, l_a was assumed to be 0.0 m. The values l_b and l_c were 4.280 and 3.195 m, respectively. It may be considered that l_c is also a decisive variable for the FOV. Obviously, the camera needs to be attached at the top of the unloading auger to obtain as large an FOV as possible. When attached to the spout, however, the camera cannot obtain a clear image because of the dust that flows out of the spout during the unloading operation. Thus, the camera was attached as close to the auger spout as possible without being obstructed by dust from the unloading operation. This position was empirically determined and regarded as constant throughout the study.

When h_c was longer than h_{kt} + h_{fr}, the associated parameters were as depicted in Fig. 4, which represents the cross-sectional view at the Y_0-Z_0 plane when θ_1 = 90°.

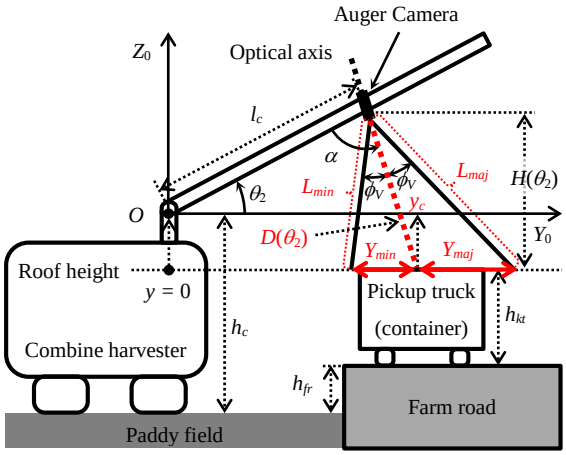

Fig. 4. Cross-sectional view at the Y_0-Z_0 plane.

The value of ϕ_V is half that of the vertical AOV. The FOV at the height of the fiducial marker on the roof is divided by the optical axis (the point y_c in Fig. 4) into two parts; the lengths of these parts along the Y_0 axis are Y_{min}, which is closer to the combine, and Y_{maj}, which is farther. L_{min} and L_{maj} are the distances between the upper or lower edges of the FOV at the roof height and optical center, respectively. The depth of field at the marker plane $D(\theta_2)$ is represented as

$$D(\theta_2) = \frac{H(\theta_2)}{\sin(\theta_2 + \alpha)} \quad (1),$$

where $H(\theta_2)$ is $l_c\sin\theta_2$ + (h_c - h_{fr} - h_{kt}). Similarly, L_{min} and L_{maj} are obtained as follows:

$$L_{min} = \frac{H(\theta_2)}{\sin(\theta_2 + \alpha - \phi_V)} \quad (2).$$

$$L_{maj} = \frac{H(\theta_2)}{\sin(\theta_2 + \alpha + \phi_V)} \quad (3).$$

Then, Y_{min} and Y_{maj} are written as follows:

$$Y_{min} = \sqrt{\{D(\theta_2)\}^2 + {L_{min}}^2 - 2D(\theta_2)L_{min}\cos\phi_V} \quad (4).$$

$$Y_{maj} = \sqrt{\{D(\theta_2)\}^2 + {L_{maj}}^2 - 2D(\theta_2)L_{maj}\cos\phi_V} \quad (5).$$

The value of y_c is obtained geometrically using Eq. (6):

$$y_c = \sqrt{\{D(\theta_2)\}^2 + {l_c}^2 - 2D(\theta_2)l_c\cos\alpha} + \frac{h_c - h_{fr} - h_{kt}}{\tan(\theta_2 + \alpha)} \quad (6).$$

Figure 5 shows the FOV and parameters that are also illustrated in Fig. 4. To make the figure clearer, the plane including the line of L_{min} and the lower edge is clipped and shown separately on the left side. Here, ϕ_H is half of the horizontal AOV. X_{min} is half of the bottom length of the rectangular triangle consisting of the angle ϕ_H and the line segment with the length L_{min}. Hence,

$$X_{min} = L_{min}\tan\phi_H \quad (7).$$

Similarly, the plane that includes the line of L_{maj} and the upper edge is depicted separately in the right side, and X_{maj} is defined along with X_{min}.

$$X_{maj} = L_{maj}\tan\phi_H \quad (8).$$

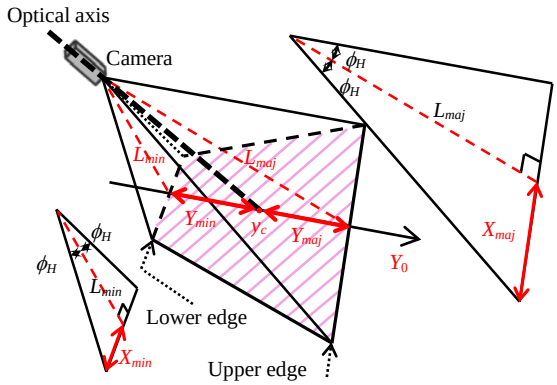

Fig. 5. Conceptual image of FOV.

Finally, the FOV can be simulated using the parameters y_c, X_{min}, X_{maj}, Y_{min}, and Y_{maj}. When h_c is shorter than h_{kt} + h_{fr}, the FOV can be simulated in a manner similar to the case of $h_c > h_{kt} + h_{fr}$.

III Auger Control for Searching Operation

Figure 6 shows the maximal FOV for the representative h_{fr} values of 0.0, 0.5, 1.0, and 1.5 m on the combine-based coordinate system (i.e., O–$X_0Y_0Z_0$ in Fig. 2) when θ_1 of the unloading auger rotates from 180° to 0°. Note that the point (X_0, Y_0) = (0, 0) in Fig. 6, which is marked as *Origin*, indicates the origin of the combine-based coordinate system. Especially for θ_1 = 0°, 90°, and 180°, the FOVs at θ_2 = 20°, 30°, 40°, and 45° have a trapezoidal shape; among them, the FOV at 20° is the narrowest and that at 45° is the widest. In short, each maximal FOV shows the total area captured by the camera when θ_2 varies from 20° to 45°. In Figs. 6(a) and (b), the maximal FOV consists of the smallest FOV at θ_2 = 20° and largest FOV at θ_2 = 45°. As shown in Figs. 6(c) and (d), the maximal FOV is only generated by the FOV at θ_2 = 45° because it includes all of the FOVs at the other θ_2 values. If searching is performed at θ_2 = 20° and θ_2 = 45°, the camera searches the total area that it can physically capture.

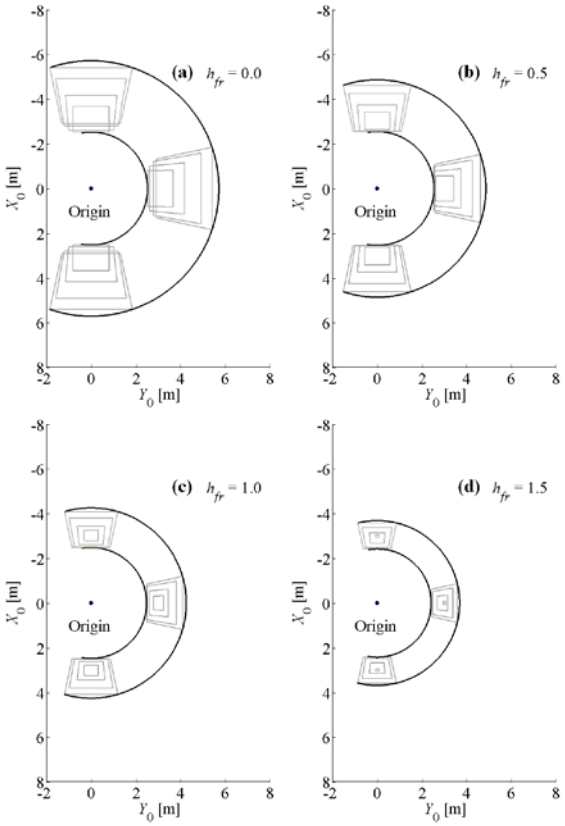

Fig. 6. Maximal FOV.
(a). h_{fr} = 0.0 m; (b). h_{fr} = 0.5 m;
(c). h_{fr} = 1.0 m; (d). h_{fr} = 1.5 m.

However, if the unloading auger rotates with θ_2 = 20°, physical interference may arise between the auger and grain storage container, especially when h_{fr} = 1.5 m. Thus, the searching procedure should be performed at θ_2 = 30° and θ_2 = 45°. Because the maximal FOV can be almost entirely covered using only the FOV at θ_2 = 45°, the searching procedure should be performed primarily

at θ_2 = 45° and then at θ_2 = 30°. Hereinafter, the former is *the primary searching step*, and the latter is *the secondary searching step*.

The entire searching procedure is as follows. First, the two joints of the unloading auger are kept at θ_1 = 192.0° and θ_2 = 2.6°, which is the state that the combine usually travels and harvests in (let this state be *the default position*). The auger moves upward to θ_2 = 45° and rotates clockwise to θ_1 = 0° (the primary step). The combine inevitably needs to keep θ_2 = 45° for the rotation from the default position to prevent the unloading auger from crashing into the cab. Then, the auger drops down to θ_2 = 30° and rotates anticlockwise to θ_1 = 90° (the secondary step). If the marker is not detected, the auger returns to the default position. During the search, only the marker detection is performed with the image processing. When the fiducial marker is detected, the auger stops immediately and rests for 2 s to obtain clearer images, which are used to calculate the precise target joint angles. After that, positioning is performed.

More than 92% of the maximal FOV can be covered by the primary step; with the additional searching by the secondary step, a coverage of more than 98% is achieved. Since the unloading auger rotates at a regular rate, the maximum times required for the primary and secondary steps are 7.9 and 4.9 s, respectively. The auger stops for 1 s to switch the searching mode from the primary step to the secondary step.

IV Field Experiment

We conducted an experiment to confirm the viability of the proposed searching-positioning method and to evaluate its efficiency. A combine robot was parked alongside a pickup truck, and a fiducial marker was placed on its roof (c.f. Fig. 1). We then ran the combine control program. The combine robot searched for the fiducial marker as described in Section III. After the marker was detected, the spout was positioned according to the basic concept. A series of searching-positioning operations was autonomously performed by the developed software program.

Two types of positional relations between the combine robot and fiducial marker were tested. In case 1, the marker was located in an area where it could be captured by the primary searching step. In case 2, the marker was located in an area where it could not be captured by the primary searching step but could be captured by the secondary searching step. We conducted the test three times for each case and recorded the angular displacement and required time for spout positioning.

For test 1 of case 1 and test 3 of case 2, the heights of the farm road h_{fr} were 2.12 and 1.06 m, respectively, whereas h_{fr} was 0.00 m in the other tests. In addition, the position and orientation of the truck relative to the combine were the same for tests 2 and 3 of case 1 and tests 1 and 2 of case 2.

V Results and Discussion

Figure 7 shows the experimental results for (a1, a2) case 1 and (b1, b2) case 2. The grey dotted line shows the locus of the auger spout during the searching process, while the red circle indicates the positioning process. The red rectangle represents the estimated position of the fiducial marker. As illustrated in Figs. 7(a1) and (b1), the primary step started its path from the default position (i.e., θ_1 = 192.0° and θ_2 = 2.6°; marked as N1 in the figure). The unloading auger raised its joint angle θ_2 up to 45° (marked as N2) and then rotated clockwise until it reached the next node N3. During this rotation, the fiducial marker was successfully detected at the spout position S1 (θ_1 = 37.5° and θ_2 = 45°). During the positioning, the auger rotated anticlockwise from S1 via S2 (θ_1 = 44.6° and θ_2 = 45°) to S3 (θ_1 = 44.6° and θ_2 = 29.8°). In this instance, it took 7.6 s for the fiducial marker to be detected. After 2.2 s of rest to obtain clearer images, the robot started the spout positioning, which took 2.0 s.

Figs. 7(b1) and (b2) show the results when the camera found the fiducial marker in the second searching step. After the end of the primary searching step (N3: θ_1 = 0° and θ_2 = 45°), the unloading auger lowered its joint angle θ_2 down to 30° (marked as N4) and then rotated anticlockwise to θ_1 = 90°. The fiducial marker was detected at the spout position S4 (θ_1 = 54° and θ_2 = 30°). After a few seconds, the auger was positioned to θ_1 = 27° and θ_2 = 0° (marked as S5). The primary searching step took 9.6 s, and it took 4.6 s from the end of the primary step for the fiducial marker to be detected. The positioning step took 3.6 s in this case. Overall, positioning took 23 s.

Table 2 summarizes the time required for the searching-positioning operation; three tests were performed for each case. The table also contains h_{fr} and the required angular displacement from the default position to the target position. Overall, θ_2 (up) was constant because the unloading auger was only raised at the beginning of the searching procedure.

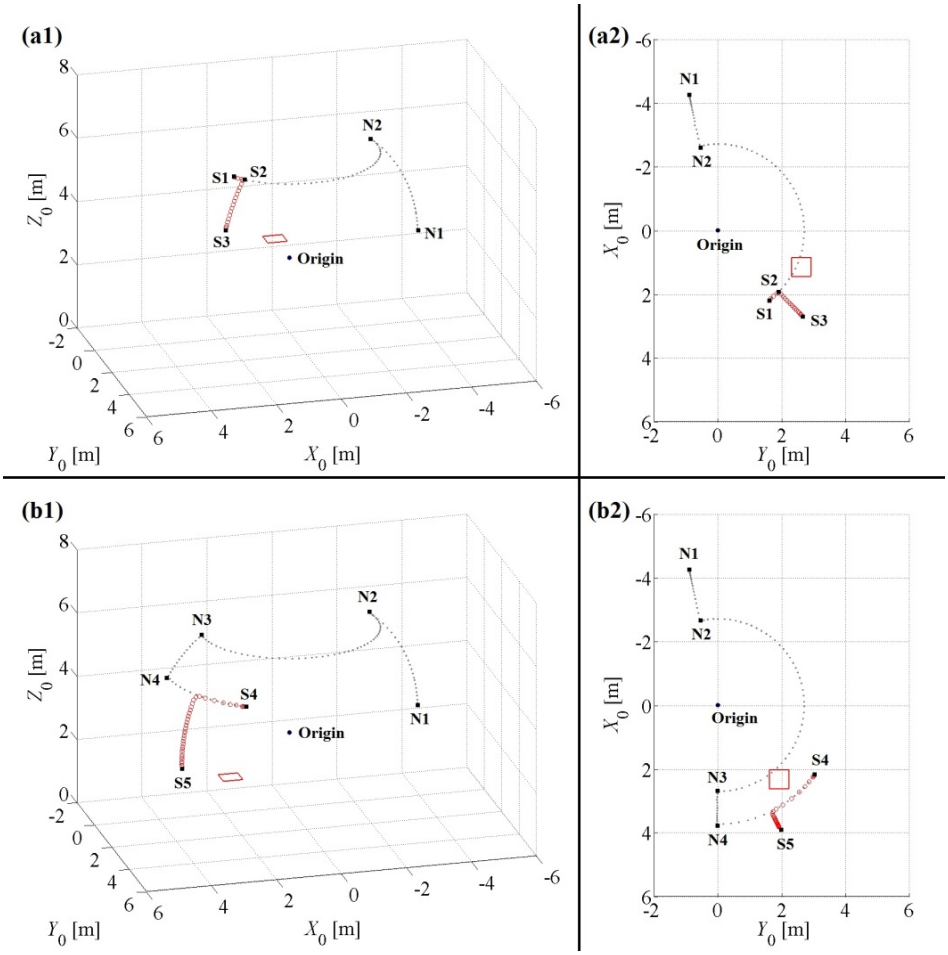

Fig. 7. Trajectory of auger spout: (a1) overhead view and (a2) top view of case 1 trajectory; (b1) overhead view and (b2) top view of case 2 trajectory.

Table 2. Required time for searching-positioning task.

Case	Test	Required time [s]	Angular displacement [°] θ_1	θ_2(up)	θ_2(down)	h_{fr} [m]
1	1	12	147.4	42.4	15.2	2.12
	2	18	133.5	42.4	45.0	0.00
	3	17	133.9	42.4	45.0	0.00
2	1	23	218.6	42.4	45.0	0.00
	2	22	216.8	42.4	45.0	0.00
	3	16	205.9	42.4	30.6	1.06
Manual operation		37 s (on average)				

For case 1, test 1 clearly required less time. h_{fr} was higher than for the other two tests with this case, and the target point was also higher. Thus, the angular displacement of θ_2 (down) was small. Compared to case 1, case 2 took longer as a whole. This is because case 2 required a larger angular displacement of θ_1. However, test 2 took 16 s, which was shorter than tests 2 and 3 of case 1. It took longer for the auger to lower its angle than in the other cases, as described in Section II-1. The difference in the required displacement of θ_2 (down) (30.6° in test 3 of case 2 while 45.0° in tests 2 and 3 of case 1) was why this test provided better results.

A combine operator took about 37 s on average to manually position the unloading auger to an appropriate point above the grain container. This is the time needed for actual unloading operation performed by not only skilled but also unskilled operators. In comparison, our proposed searching-positioning method is clearly more efficient (18 s on average). As noted in Section III, the primary searching step covers most of the maximal FOV. In other tests we conducted, the marker was usually detected in this step. Thus, the secondary step serves as an auxiliary searching procedure. However, the addition of the second step allows the auger camera to cover 98% of the maximal FOV.

VI Summary

In order to realize efficient marker searching operation, the FOV of an auger camera was computed on the basis of decision variables associated with the FOV. Under the assumption that the marker is searched for by the auger camera, we proposed an efficient marker searching procedure on the basis of the simulation results.

The maximal FOVs at representative θ_2 values were computed. The simulation results indicated that 92% of the maximal FOV can be covered by searching at θ_2 = 45° (the primary searching step), and 98% of the maximal FOV is covered by also searching at θ_2 = 30° (the secondary searching step). The experimental results showed that the fiducial marker was mainly detected in the primary searching step. The secondary searching step was still useful for achieving the maximal FOV. The fiducial marker was detected when located inside the maximal FOV either during the primary or secondary searching step; additional searching steps were not needed. The combine robot accurately recognized the marker with the auger camera while rotating its unloading auger and then positioned its spout at the target point on the basis of the detected marker.

When the fiducial marker was detected in the primary searching step, the robot took 16 s on average for searching and positioning. It took 20 s on average when the fiducial marker was acquired in the secondary step. With the proposed method, the combine robot performed the searching-positioning task within 18 s on average, which is less than the time required for manual operation.

Therefore, the combine robot can use the proposed method to search, detect, and position with high efficiency and sufficient reliability.

References

Buckmaster, D. R. and Hilton, J. W. 2005. Computerized cycle analysis of harvest, transport, and unload systems. Computer and Electronics in Agriculture 47: 137-147.

Gonzalez, R. C. and Wintz, P. 1987. Digital Image Processing 2nd Edition. Addison-Wesley Publishing Company, MA, USA.

Iida, M., Uchida, R., Zhu, H., Suguri, M., Kurita, H. and Masuda, R. 2013. Path-following control for a head-feeding combine robot. Engineering in Agriculture, Environment and Food 6(2): 61-67.

Ishida, M., Imou, K., Okado, A., Takenaga, H., Honda, Y., Itokawa, N. and Shibuya, Y. 1998. Autonomous tractor for forage production. Journal of the Japanese Society of Agricultural Machinery 60(2): 59-66.

Kurita, H., Iida, M., Suguri, M. and Masuda, R. 2012. Application of Image Processing Technology for Unloading Automation of Robotic Head-Feeding Combine Harvester. Engineering in Agriculture, Environment and Food 5(4): 146-151.

Nagasaka, Y., Umeda, N., Kanetani, Y., Taniwaki, K. and Sasaki, Y. 2004. Automated rice transplanter using global positioning and gyroscopes. Computer and Electronics in Agriculture 43: 223-234.

Noguchi, N. and Terao, H. 1997. Path planning of an agricultural mobile robot by neural network and genetic algorithm. Computer and Electronics in Agriculture 18: 187-204.

Salaris, P., Pallottino, L., Hutchinson, S. and Bicchi, A. 2011. From Optimal Planning to Visual Servoing with Limited FOV. In Proc. 2011 IEEE/RSJ International Conference on Intelligent Robots and Systems, 2817-2824. San Francisco, CA., 25-30 September.

Takai, R., Barawid, O. Jr., Ishii, K. and Noguchi, N. 2010. Development of Crawler-Type Robot Tractor based on GPS and IMU. Preprint of the IFAC International Conference on AGRICONTROL 2010, A3-5. Kyoto, Japan, 6-8 December.

Tsotsos, J. K. and Shubina, K. 2007. Attention and Visual Search: Active Robotic Vision Systems that Search. Keynote Lecture of the 5th International Conference on Computer Vision Systems, Bielefeld, Germany, 21-24 May.

Xu, G. and Zhang, Z. 1996. Epipolar Geometry in Stereo, Motion and Object Recognition: A Unified Approach. Norwell: Kluwer Academic Publishers.

Zhang, H. and Ostrowski, J. P. 2002. Visual Motion Planning for Mobile Robots. IEEE Transactions on Robotics and Automation 18(2), 199-208.